Optics & Laser Technology 141 (2021) 107175

Contents lists available at ScienceDirect

Optics and Laser Technology

journal homepage: www.elsevier.com/locate/optlastec

Full length article

A free-running dual-comb spectrometer with intelligent temporal alignment algorithm

Qiuquan Yan [a,1], Yiming Li [b,1], Jun Zhang [a], Xin Zheng [c], Dan Wu [a,d], Ke Yin [c], Tian Jiang [b,e,*]

[a] College of Computer, National University of Defense Technology, Changsha 410073, China
[b] College of Advanced Interdisciplinary Studies, National University of Defense Technology, Changsha 410073, China
[c] National Innovation Institute of Defense Technology, Academy of Military Sciences PLA China, Beijing 100071, China
[d] Hefei Interdisciplinary Center, National University of Defense Technology, Hefei 230037, China
[e] Beijing Institute for Advanced Study, National University of Defense Technology, Beijing 100020, China

ARTICLE INFO

Keywords:
Dual-comb spectrometer
Fiber laser
Absorption spectroscopy
Back-propagation

ABSTRACT

Dual-comb spectrometer is demonstrated as a promising tool in atmospheric composition detection with extremely-high spectral resolution and fast scanning capability. In this paper, an intelligent temporal alignment (ITA) algorithm is proposed into signal processing of a free-running dual-comb spectrometer around 1.5 μm. The signal processing in the algorithm only relies on the original interference sequence to complete the signal alignment without reference signal. As a result, the alignment of ^{12}CO gas absorption line in the wavelength range of 1564-1570 nm is well retrieved in good agreement with HITRAN database. To the best of our knowledge, this paper proposes and implements for the first time the combination of the ITA algorithm and free-running dual-comb spectroscopy. It lays a technical foundation for the intelligent analysis of arbitrary gas absorption spectral lines.

1. Introduction

In recent years, there have been more and more researches on applying machine learning methods to optics and photonics [1–4]. In the field of ultrafast photonics, machine learning technology accelerates the research in optical communications [5], quantum optics [6], and super-resolution microscopy [7]. Optical frequency comb (OFC) effectively links the optical frequency and microwave frequency in the electromagnetic spectrum, providing a high-precision frequency source in a simple and ingenious way [8,9]. With the continuous evolution of OFC, optical absorption spectroscopy develops rapidly, of which dual comb spectroscopy (DCS) has attracted the most attentions [10–12]. Relying on dual-path optical combs as the core, DCS brings parallel multi-heterodyne detection, avoiding mechanical scanning with high frequency resolution and rapid sampling rate [13]. When the research of DCS is combined with machine learning, its development may be accelerated. The signal analysis of DCS is an important direction in DCS technology. Machine learning has great advantages in the processing and analysis of large datasets [14], which happens to solve the problem of the large amount of spectral signal data in the DCS system.

With the development of DCS, a single cavity free-running DCS system appears as an attractive structure which only requires a single resonator in free-running. It simultaneously generates two sets of pulse sequences which have a stable difference in repetition frequency. Besides, it does not require any external locking, and can be directly used for dual-comb spectral detection [15]. So far, polarization multiplexing [12,16,17], wavelength multiplexing [18–20], and directional multiplexing [21,22] free-running single cavity dual-comb light sources have been used widely in gas detection such as CH_4, H_2O and etc. [23]. In contrast, directional multiplexing can directly generate two spectrally overlapped soliton mode-locked pulses in the clockwise (CW) and counterclockwise (CCW) directions without additional nonlinear frequency broadening.

Despite its many advantages, there are still some problems in processing gas absorption signal. Because of the low signal-to-noise ratio (SNR) of a single interferogram, it is necessary to collect multiple interferograms for analysis. Moreover, although the single cavity DCS has the ability of common-mode noise elimination, correction algorithms are still needed to distinguish fine spectral lines. The misalignment between adjacent interference signals (i.e. the beat signals of the two

* Corresponding author at: Beijing Institute for Advanced Study, National University of Defense Technology, Beijing 100020, China.
E-mail address: tjiang@nudt.edu.cn (T. Jiang).
[1] These authors contributed equally to this paper.

https://doi.org/10.1016/j.optlastec.2021.107175
Received 5 December 2020; Received in revised form 14 March 2021; Accepted 19 April 2021
Available online 1 May 2021

optical combs) makes it difficult to retrieve the gas absorption characteristics in the time domain.

Previous work has shown that the DCS interference signal can be described as [24]

$$x(t) = \sum_{n=0}^{N-1} A_n e^{i(\phi_0(t)+n\Delta\phi(t))} \quad (1)$$

where $x(t)$ is the measured interference signal, A_n is the amplitude of nth line. $\phi_0(t)$ and $\Delta\phi(t)$ correspond to carrier envelope offset phase and repetition frequency phase at time t respectively. Essentially the change of $\phi_0(t)$ and $\Delta\phi(t)$ causes the instability of interference signal.

In 2016, an computational correction method of DCS was proposed by Burghoff et al. [24] which restored the time domain and frequency domain characteristics of the interference signal. 2 years later, Guay et al. [25] realized the correction of the interference signal collected by the electro-optic dual-comb system (EODCS) by using custom post-correction software, and successfully restored the $H^{13}CN$ absorption spectrum. Fdil et al. [26] applied the pseudo-random binary sequence phase modulation to the EODCS in 2019, and realized real-time correction of the phase of the resampled interference signal by recording the periodic change information of the interference signal phase. Sterczewski et al. [27] proposed a computational coherent averaging algorithm to realize real-time correction of interference signals. They deploy the algorithm in FPGA, reducing the dependence on the DCS system. Another approach designed by Sterczewski et al. [28] was named all-computational phase retrieval and correction algorithm. It was used to find the position of the endpoint in the interference signal envelope. The interference signal was resampled using the position as the trigger point. Most of the methods proposed above are based on cross-correlation analysis (CCA) or similar ideas to offset the phase of the interference signal to achieve signal alignment. But these algorithms inevitably require frequency-domain information or secondary sampling to correct the interference signal. The CCA method is suitable for the correction of interference signals in a relatively stable DCS system. Some DCS systems are weak in stability and cannot ensure the coherence of the dual comb within one interference signal generation period. CCA makes it difficult to correct the signals in these systems. To resolve the problem that the interference signal cannot be corrected by shifting the phase in the DCS system, a new machine learning algorithm called intelligent temporal alignment (ITA) algorithm is first proposed for alignment and noise reduction of dual-comb interference signals.

In this paper, a free-running dual-comb spectrometer based on a single-cavity bidirectional mode-locked fiber laser [29] is built that runs stably for a long time. It remains stable bidirectional mode-locking over 9 hours in a free-running scheme with a repetition frequency difference of only 64 Hz. It is applied to detect ^{12}CO in near-infrared region. Additionally, the ITA algorithm gives the similar functionality in terms of correcting on $\phi_0(t)+n\Delta\phi(t)$ in Eq. (1), but just needs the interference signal in the time domain, no reference signal nor secondary sampling. Referring to the trainable time warping (TTW) [30], neural time warping (NTW) [31] and other machine learning algorithms [32,33], the proposed ITA algorithm abstracts the interference signal correction problem into the parameter optimization problem, and applies the back-propagation method commonly used in the field of machine learning. The TTW and NTW algorithms proposed in [30,31] applied the traditional machine learning algorithm model to achieve the alignment of the speech time series. The deep neural network algorithms proposed in [32,33] realized the spectral response prediction and reverse design of two-dimensional materials by establishing appropriate network model. Compared with the reference algorithms, the ITA algorithm uses a completely different rational quadratic (RQ) kernel function for the signal fitting recovery in the forward propagation phase. The experimental results show that the algorithm can well correct the gas absorption spectrum in terms of frequency and line shape as well as successfully retrieve the absorption spectrum of ^{12}CO in the 1564-1570 nm band, which is in good agreement with HITRAN database [34]. The experiment setup of free-running dual-comb spectrometer is presented in Section 2. The details of the ITA algorithm are described in Section 3. Experiment results and discussion are shown in Section 4. At last, the main conclusions of this work are summarized in Section 5.

2. Free-running dual-comb spectrometer

The dual-comb spectrometer setup is seeded by an all-fiber single cavity bidirectional mode-locked laser [35], sketched in Fig. 1 (a). The laser consists of a wavelength division multiplexer (WDM), a piece of 0.36 m Er fiber (110-4/125) served as gain medium pumped by a 980 nm laser diode, a polarization controller (PC) used to change the intracavity polarization evolution, a fiber saturable absorber (SA) based on single-walled carbon nanotube saturable absorber (SWCNT) film, and a four-port 10/90 optical coupler (OC). The 90% port of the optical power was fed back into the cavity, while 10% used for laser output. The total length of the cavity is ~3.78 m, and the laser is equipped with a fine temperature control. Fig. 1(b) shows the stability of the bidirectional output frequency acquired at 1s gate time. By monitoring the two output channels of the laser, it is found that it can maintain stable for more than 9 hours in a free-running scheme. The jitter range of the repetition frequency difference is about 10 Hz (see black curve in Fig1. (b)). The inset of Fig. 1(b) reflects that the standard deviation of the repetition frequency difference in the system accounts for 2.83% of the mean value, which indicates that the spectrometer cannot be applied directly to gas detection without any signal correction.

The realization of mode-locking is based on a typical SA mode-locking mechanism [36]. The laser operates in the anomalous dispersion regime, generating soliton pulses with pulse widths of 810 fs and 687 fs for the CW and CCW direction, respectively, at 52.29 MHz repetition frequency. The output powers are 295 μW for CW and 322 μW for CCW pulses, correspondingly. As shown in Fig. 1(c), the spectrum shows that laser behaves in a typical soliton mode-locked state.

In the ensuing two arms of the spectroscopy setup, the pulses are first coupled by a 50/50 OC. Then, one of the outputs, named signal path, is transmitted through an 80 cm-long gas cell applied with 300 Torr ^{12}CO and 300 Torr ^{13}CO mixture, while the other path is placed in parallel to the sample path, to provide a reference signal without the gas absorption. To compensate the large inserted loss of gas cell, the signal path is launched into an Er-doped fiber amplifier with a maximum output power of 23 dBm firstly. After that, a 2 μm InGaAs photodetector (PD) is used to detect the dual-comb interferogram followed by a DC isolator with a detection range of 0.1-500 MHz, a 32 MHz low-pass filter, and an electrical amplifier. We refer to these components collectively as electrical signal optimization devices (ESOD) in Fig. 1(a). Finally, the interferogram signal is monitored and recorded by an oscilloscope with a bandwidth of 1 GHz.

3. Intelligent temporal alignment algorithm

The noises of the collected interference signal mainly consist of two parts, namely additive amplitude noise (AAN) and multiplicative phase noise (MPN). AAN can be reduced coherently by a large number of interference signals, while MPN needs to be reduced by carrier and time recovery algorithms. Unlike those approaches that require secondary sampling to extract the correction signal, the ITA algorithm is based entirely on the original time domain interference signals to achieve the attenuation of the noises. The ITA algorithm is illustrated in Fig. 2 which is based on the back-propagation method. The ITA algorithm is adopted for blind correction of phase fluctuations, and constantly optimize the offset parameters by shifting the strength and position of each sampling point in the interference signal, so as to minimize the differences among all interference sequences.

The correction problem of interference signal can be formally described as follows: The acquired N interference signals X of T length (i.

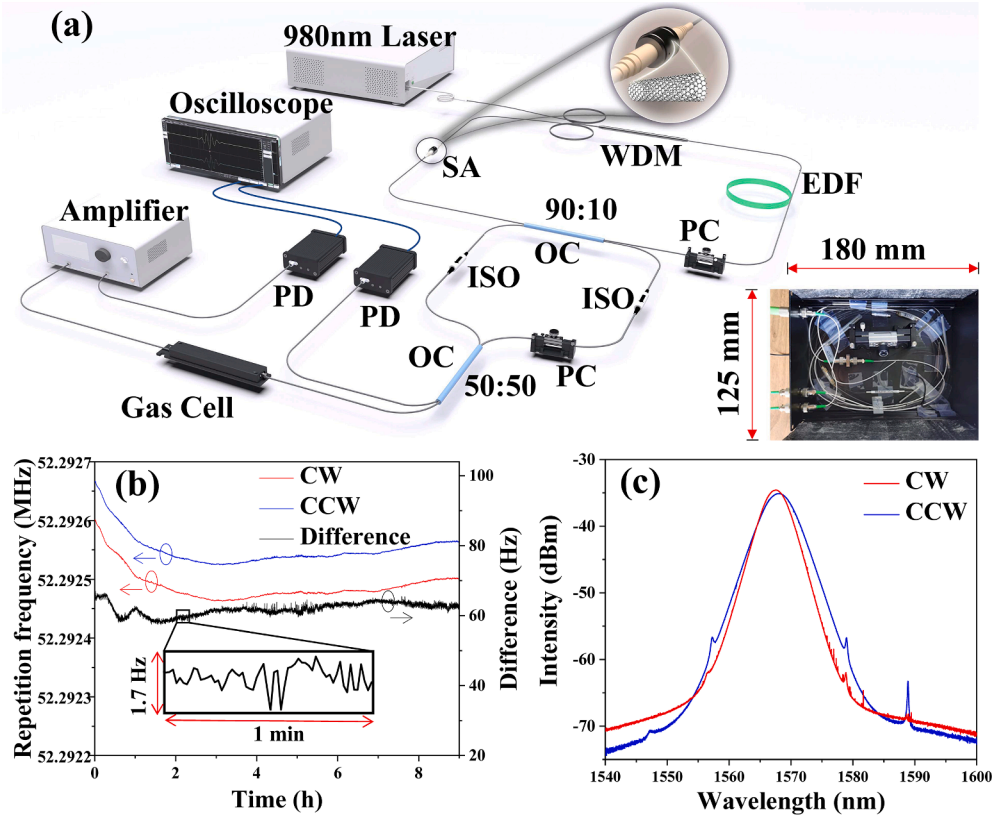

Fig. 1. Setup of the dual-comb spectrometer. (a) The structure of the bidirectional mode-locked fiber laser. WDM, 980/1560 nm wavelength division multiplexer; PC, polarization controller; SA, saturable absorber; OC, optical coupler; ISO, isolator; PD, photodetector; ESOD: electrical signal optimization devices, from left to right are DC isolator, low-pass filter and electrical amplifier. The inset in the lower right corner indicates the mode-locked fiber laser. (b) The stability of repetition frequency in bidirectional outputs (red and blue) and the variation of the repetition frequency difference (black). The inset represents the variation of the repetition frequency difference within 1 minute. (c) The spectrums of bidirectional outputs.

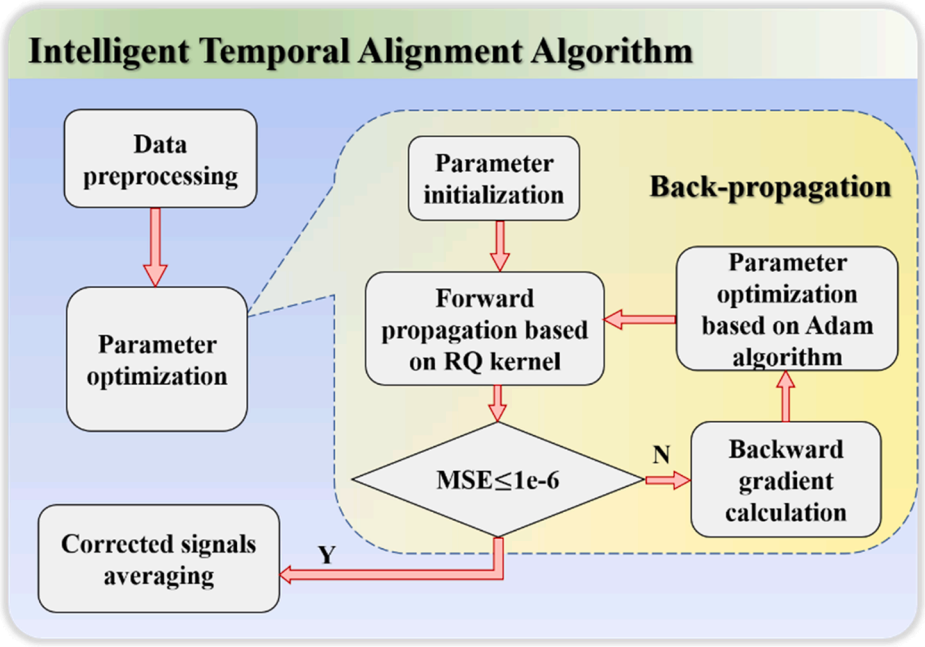

Fig. 2. The flowchart of intelligent temporal alignment algorithm.

e., $X = [x_1, \cdots, x_N]$ where $x_n = [x_n[1], \cdots, x_n[T]]$) represents the discrete signal. In the data preprocessing stage, the continuous collected interference signal is divided into several single interferograms expressed in X. When the dual-comb spectrometer keeps in the ideal situation, that is, $\phi_0(t)$ and $\Delta\phi(t)$ remain unchanged, all the interference signals collected should be completely consistent. Therefore, the proposed goal in this problem is to align all interference sequences so that the differences in shape and intensity between them are as small as possible. A within-group mean square error (MSE) is applied to measure the difference between interference signals. Symbol $X^{'}$ is employed to represent the interference signal aligned by the algorithm, whose magnitude is consistent with that of original series X. The corresponding MSE expression is

$$D(X^{'}) = \frac{1}{NT}\sum_{n=1}^{N}\sum_{t=1}^{T}(x^{'}{}_{n}[t] - y[t])^{2},$$
$$y[t] = \frac{1}{N}\sum_{n=1}^{N}x^{'}{}_{n}[t] \tag{2}$$

where y represents the direct averaging signal of the interference sequence after alignment.

In the process of aligning interference, each sampling point is adjusted in the original interference signal. Therefore, the RQ kernel function is introduced as convolution kernel in ITA algorithm to realize proper correction of sampling points. The expression for the RQ function is

$$RQ(t) = \left(1 + \frac{t^2}{2\alpha l^2}\right)^{-\alpha} \tag{3}$$

where α and l are set to 1 and 2.

In addition, in order to realize the nonlinear offset correction of time series, the mapping from interference sequences X to X' has to be given. Let [1, …, T] be the timing of X, and $\tau_n = [\tau_n[1], \ldots, \tau_n[T]]$ be the timing of X'. The mapping relationship between the two is set as

$$\tau_n[t] = t + \sum_{k=1}^{K} b_k^n \sin\left(\frac{k(t-1)}{T-1}\right) \tag{4}$$

where K is the number of learning parameter defined manually, and $\boldsymbol{b^n} = [b_1^n, \cdots, b_K^n]$ are the parameters to be optimized for τ_n. By utilizing the RQ convolution kernel, the conversion equation from X to X' is

$$x^{'}{}_{n}[t] = \sum_{m=\lfloor\tau_n[t]\rfloor-40}^{\lfloor\tau_n[t]\rfloor+40} x_n[m]RQ(\lfloor\tau_n[t]\rfloor - m) \tag{5}$$

where $\lfloor\tau_n[t]\rfloor$ denotes the integer rounded down by $\tau_n[t]$. This equation is the core of nonlinear correction for interference signal sampling points. When the undetermined parameters in Eq. (4) reach the optimal value, the X' obtained through Eq. (5) is the interference signal after nonlinear deviation. Therefore, the final corrected interference signal y can be calculated by averaging of X' in Eq. (2).

An optimal set of B (i.e., $B = [\boldsymbol{b}^1, \cdots, \boldsymbol{b}^n]$) is estimated by numerically solving the optimization problem using back-propagation method:

$$\widehat{B} = \underset{B}{\operatorname{argmin}} D(X^{'}) \quad s.t. \begin{cases} 0 \le \Delta\tau_n[t] \le 1 \;\; t \in \{2, \cdots, T\} \\ \tau_n[1] = 1, \;\; \tau_n[T] = T \end{cases} \tag{6}$$

where the function of distance sequences D(X') is the within-group MSE of time-series X' and $\Delta\tau_n[t] = \tau_n[t] - \tau_n[t-1]$. The constraints in this function correspond to the dynamic time warping constraints [37] which are used to ensure the correctness and effectiveness of the algorithm in the process of correcting signals.

In the back-propagation process of ITA algorithm, the execution process of the algorithm is illustrated according to the order of forward propagation, backward gradient calculation and parameters updating. The value of K is set to 32 in the parameter initialization phase. Because the interference signals are not well corrected when the value is too small, as well as the computational overhead is too high to be acceptable once the value is too large. Meanwhile, all the parameters of matrix B are initialized to 0 to minimize the search space for the parameters.

In the forward propagation phase, the aligned interference X' is calculated by using Eq. (3)-(5) from the original sequence X and the matrix B. The distance $D(X')$ between the corrected sequence and the average interference signal y can be calculated by Eq. (2). At the backward gradient calculation stage, the gradient of $D(X')$ is calculated by computing the derivative of distance $D(X')$ with respect to B. In the last part, Adam algorithm [38] is used to update the parameters of matrix B. The main advantage of Adam algorithm lies in its ability to design independent adaptive learning rates for different parameters, so that the results can converge faster. At last, the corrected signal y is calculated by averaging the X'.

4. Result and discussion

As shown in Fig. 3, three types of interferograms are compared. In the experiment, the acquisition time was set to 2 s and the sampling rate was 100 MS/s. The 1 ms signal is extracted from the continuous collected interference signal as a single interferogram, and its center position is set as the peak. Fig. 3(a), (c) and (e) show the single interference signal, the signal averaging 240 times of the interference signal, and the interference signal corrected by the ITA algorithm using 120 interferograms under the 1 ms time window, respectively. The SNR of the single interference is too low to distinguish any gas absorption in the frequency spectrum. The average results show a low absorption spectral resolution and shallow dips of gas absorption in Fig. 3(d). This proves that the average method is not applicable to our bidirectional free-running dual-comb spectrometer. By combining the detection platform with the algorithm, this paper basically realized the detection of gas absorption spectral line of ^{12}CO.

Fig. 4(a) shows the interference signals under 0.006 ms in detail. Compared to the single signal, the interference signal noise corrected by different method has a significant attenuation. By means of average method and algorithm correction, the SNR of the interferogram is increased by ~4.79 dB and ~42.72 dB in the time domain respectively. In the result of average method, although the position of the gas absorption in the radio spectrum is reflected, the absorption intensity is weak. Furthermore, several additional tiny absorptions around each absorption line lead to the decrease of frequency resolution as well as the deterioration of the linewidth. These indicate that the condition of the dual-comb spectrometer has not been stable during the process of data collecting. Therefore, the average method cannot fundamentally solve the problem of spectrum drift of interferogram. After the correction of the ITA algorithm, the misalignment of interferogram in time domain has been ameliorated, thus the gas absorption in frequency domain has been improved. Fig. 4(b) shows the free induction decay signal (FID) in the interference signal corrected by ITA algorithm. It is the main component that reflects the dips of the gas absorption spectrum, which has been confirmed previously [39]. However, the FID signal could not be observed in the single interference signal and the averaging interference signal in Fig. 3(a) and (c). Besides, the clear absorption lines cannot be seen in the frequency spectrum of averaging interference signal through fast Fourier transform. By shifting the position and intensity of each sampling point in the interference signals, the ITA algorithm corrects the fluctuation and makes up for the shortcoming of the average method.

When comparing with the HITRAN standard database, only ^{12}CO in the gas cell has certain absorption in the 1564-1570 nm. Fig. 4(c) shows the comparison of the gas absorption spectrum between average, ITA algorithm correction and HITRAN database. Because the gas cell is a mixture of ^{12}CO and ^{13}CO isotopes, the absorption spectrum is weaker than the single CO gas. Furthermore, the DCS system has great fluctuations in the repetition frequency difference. As shown in Fig 1(b), the DCS system maintains an average repetition frequency difference of 64 Hz, but its fluctuation range reaches 10 Hz. Thus, the detection is more challengeable. In the result of average, there are only 6 visible absorption lines. The linewidth of the absorption spectrum corrected by ITA algorithm is less than the average result. Result in this paper shows that the gas absorption spectrum corrected by the algorithm can basically correspond to the position, shape and normalized intensity of the ^{12}CO absorption spectrum in HITRAN. Fig. 4(d) shows the details of the absorption spectrum at 1569.54 nm. The shape of the spectrum corrected by the algorithm in the experiment is consistent with the database.

Fig. 5 shows the corresponding normalized gas absorption spectrum after the interference signal which was corrected by ITA algorithm. The position of the central wavelength of the absorption spectrum is inferred

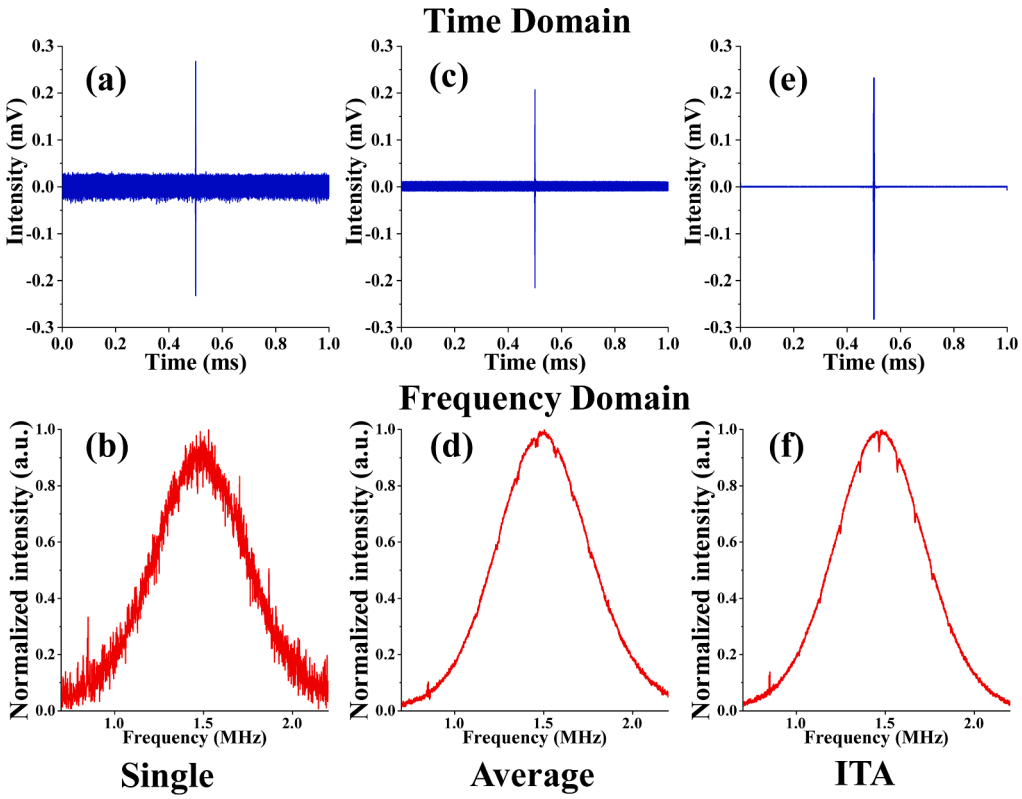

Fig. 3. Comparison of interference signals in time and frequency domain. From left to right: single signal, averaged signal and the signal corrected by ITA algorithm. In each column, the top rows show the time domain signal within 1 ms laboratory time, and the bottom plots are the frequency domain signal.

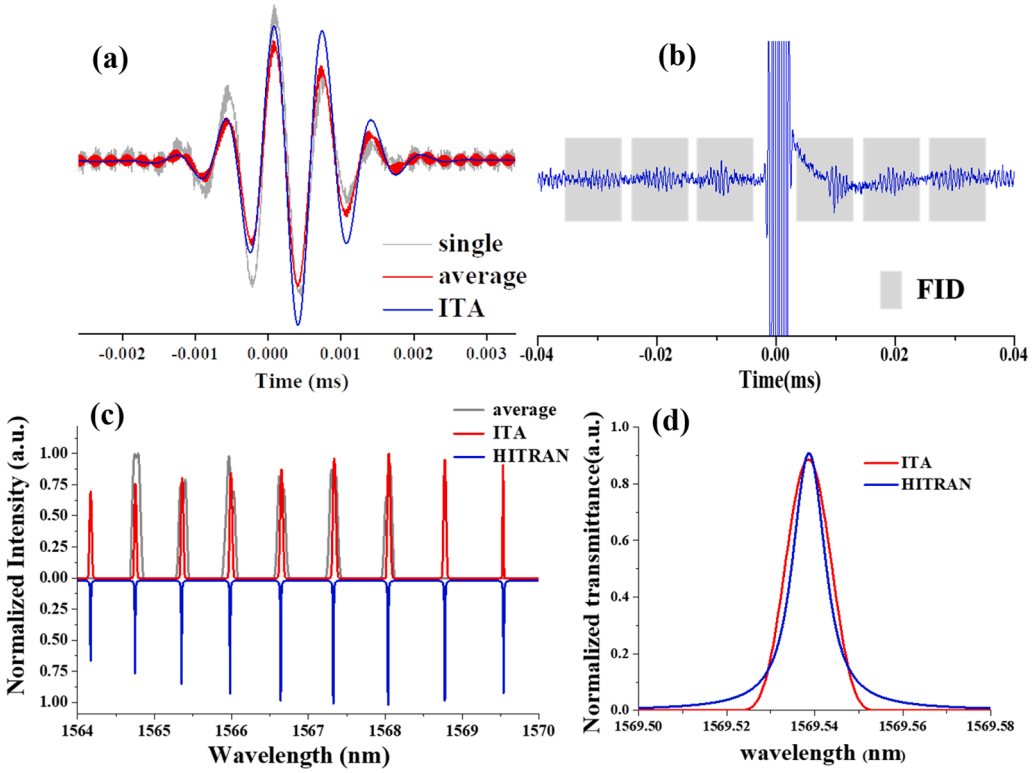

Fig. 4. Comparison of interference signal and absorption spectrum before and after ITA algorithm correction. (a) Time domain comparison in detail. (b) The free induction decay (FID) signal in the interference signal corrected by ITA algorithm. (c) The comparison of gas absorption normalized spectrum between average, algorithm correction and ^{12}CO absorption spectrum in HITRAN database at 1564-1570 nm. (d) The magnified result at 1569.54 nm in (c).

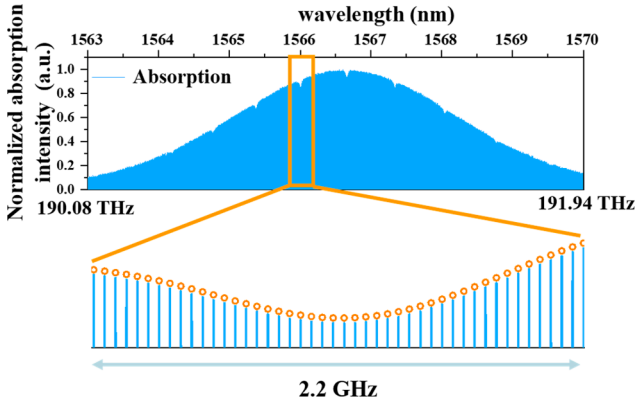

Fig. 5. ^{12}CO gas absorption spectrum after ITA algorithm correction.

by the spectrum shown in Fig. 1(c). According to the conversion equation [28] from the radio frequency to optical frequency, the radio spectrum of the system is 1-2 MHz, corresponding to the 1564-1570 nm in optical domain. Within this range, there are 9 locations with significant gas absorption. The manifest area corresponds to the wavelength position of 1566 nm, and the absorption frequency range is about 2.2 GHz. In the result of ITA algorithm correction, the recovered gas absorption linewidth is slightly wider than the standard line in HITRAN. It can be attributed to that the structure of the ITA algorithm is not adequate enough. The main challenge in ITA algorithm is that the collected samples are discrete, which naturally leads to the loss of precision, resulting in roundoff errors in the correction process.

5. Conclusion

In this paper, a 1.5 μm free-running dual-comb spectrometer was set up. This work proposed for the first time that the ITA algorithm can be used to process the dual-comb spectrum data, which provides a new idea for the study of weak spectral absorption signals. Through algorithm correction, the absorption spectrum information of ^{12}CO gas in the range of 1564-1570 nm was successfully retrieved. The experiment results were in consistent with the HITRAN database in the frequency position, spectral line intensity and shape. The combination of dual-comb spectrometer and ITA algorithm is beneficial to the miniaturization design of gas detection structure. In the future, the accuracy of the ITA algorithm can be improved by modifying kernel function or increasing the complexity of the algorithm. In this way, the linewidth of absorption spectrum can be optimized. It is believed that the presented bidirectional free-running dual-comb spectrometer with ITA algorithm can be implemented to achieve broadband absorption detection in the near future.

Funding

This work was supported by the National Natural Science Foundation of China (NSFC) [11804387, 11802339, 11805276, 11902358, 61805282, 61801498, 62075240]; the Scientific Researches Foundation of National University of Defense Technology [ZK18-03-22, ZK18-01-03, ZK18-03-36]; and the Science Fund for Distinguished Young Scholars of Hunan Province [2020JJ2036].

Declaration of Competing Interest

The authors declare that they have no known competing financial interests or personal relationships that could have appeared to influence the work reported in this paper.

References

[1] X. Xu, M. Tan, B. Corcoran, J. Wu, A. Boes, T.G. Nguyen, S.T. Chu, B.E. Little, D. G. Hicks, R. Morandotti, A. Mitchell, D.J. Moss, 11 TOPS photonic convolutional accelerator for optical neural networks, Nature 589 (2021) 44–51.
[2] J. Feldmann, N. Youngblood, M. Karpov, H. Gehring, X. Li, M. Stappers, M. Le Gallo, X. Fu, A. Lukashchuk, A.S. Raja, J. Liu, C.D. Wright, A. Sebastian, T. J. Kippenberg, W.H.P. Pernice, H. Bhaskaran, Parallel convolutional processing using an integrated photonic tensor core, Nature 589 (2021) 52–58.
[3] B.J. Shastri, A.N. Tait, T. Ferreira de Lima, W.H.P. Pernice, H. Bhaskaran, C. D. Wright, P.R. Prucnal, Photonics for artificial intelligence and neuromorphic computing, Nat. Photonics 15 (2021) 102–114.
[4] G. Genty, L. Salmela, J.M. Dudley, D. Brunner, A. Kokhanovskiy, S. Kobtsev, S. K. Turitsyn, Machine learning and applications in ultrafast photonics, Nat. Photonics (2020).
[5] D. Zibar, M. Piels, R. Jones, C.G. Schäeffer, Machine Learning Techniques in Optical Communication, J. Lightwave Technol. 34 (2016) 1442–1452.
[6] A.M. Palmieri, E. Kovlakov, F. Bianchi, D. Yudin, S. Straupe, J.D. Biamonte, S. Kulik, Experimental neural network enhanced quantum tomography, npj Quant. Inform. 6 (2020) 20.
[7] A. Durand, T. Wiesner, M.-A. Gardner, L.-É. Robitaille, A. Bilodeau, C. Gagné, P. De Koninck, F. Lavoie-Cardinal, A machine learning approach for online automated optimization of super-resolution optical microscopy, Nat. Commun. 9 (2018) 5247.
[8] T. Fortier, E. Baumann, 20 years of developments in optical frequency comb technology and applications, Commun. Phys. 2 (2019).
[9] S.A. Diddams, K. Vahala, T. Udem, Optical frequency combs: Coherently uniting the electromagnetic spectrum, Science 369 (2020).
[10] N. Picqué, T.W. Hänsch, Frequency comb spectroscopy, Nat. Photonics 13 (2019) 146–157.
[11] X. Zhao, Z. Zheng, Y. Liu, G. Hu, J. Liu, Dual-Wavelength, Bidirectional Single-Wall Carbon Nanotube Mode-Locked Fiber Laser, IEEE Photon. Technol. Lett. 26 (2014) 1722–1725.
[12] X. Zhao, T. Li, Y. Liu, Q. Li, Z. Zheng, Polarization-multiplexed, dual-comb all-fiber mode-locked laser, Photon. Res. 6 (2018) 853–857.
[13] I. Coddington, N. Newbury, W. Swann, Dual-comb spectroscopy, Optica 3 (2016).
[14] J. Zhou, B. Huang, Z. Yan, J.-C.G. Bünzli, Emerging role of machine learning in light-matter interaction, Light: Sci. Appl. 8 (2019) 84.
[15] M.I. Kayes, N. Abdukerim, A. Rekik, M. Rochette, Free-running mode-locked laser based dual-comb spectroscopy, Opt. Lett. 43 (2018) 5809–5812.
[16] Y. Nakajima, Y. Hata, K. Minoshima, All-polarization-maintaining, polarization-multiplexed, dual-comb fiber laser with a nonlinear amplifying loop mirror, Opt. Express 27 (2019) 14648–14656.
[17] Z. Deng, Y. Liu, C. Ouyang, W. Zhang, C. Wang, W. Li, Mutually coherent dual-comb source generated from a free-running linear fiber laser, Results Phys. 14 (2019), 102364.
[18] Z. Luo, A. Luo, W. Xu, H. Yin, J. Liu, Q. Ye, Z. Fang, Tunable Multiwavelength Passively Mode-Locked Fiber Ring Laser Using Intracavity Birefringence-Induced Comb Filter, IEEE Photon. J. 2 (2010) 571–577.
[19] X. Zhao, G. Hu, B. Zhao, C. Li, Y. Pan, Y. Liu, T. Yasui, Z. Zheng, Picometer-resolution dual-comb spectroscopy with a free-running fiber laser, Opt. Express 24 (2016) 21833–21845.
[20] R. Liao, Y. Song, W. Liu, H. Shi, L. Chai, M. Hu, Dual-comb spectroscopy with a single free-running thulium-doped fiber laser, Opt. Express 26 (2018) 11046–11054.
[21] K. Kieu, M. Mansuripur, All-fiber bidirectional passively mode-locked ring laser, Opt. Lett. 33 (2008) 64–66.
[22] J. Olson, Y. Ou, A. Azarm, K. Kieu, Bi-directional mode-locked thulium fiber laser as a single-cavity dual-comb source, IEEE Photon. Technol. Lett. 30 (2018) 1772–1775.
[23] J. Chen, X. Zhao, Z. Yao, T. Li, Q. Li, S. Xie, J. Liu, Z. Zheng, Dual-comb spectroscopy of methane based on a free-running Erbium-doped fiber laser, Opt. Express 27 (2019) 11406–11412.
[24] D. Burghoff, Y. Yang, Q. Hu, Computational multiheterodyne spectroscopy, Sci. Adv. 2 (2016), e1601227.
[25] P. Guay, J. Genest, A.J. Fleisher, Precision spectroscopy of H(13)CN using a free-running, all-fiber dual electro-optic frequency comb system, Opt. Lett. 43 (2018) 1407–1410.
[26] K. Fdil, V. Michaud-Belleau, N.B. Hebert, P. Guay, A.J. Fleisher, J.D. Deschenes, J. Genest, Dual electro-optic frequency comb spectroscopy using pseudo-random modulation, Opt. Lett. 44 (2019) 4415–4418.
[27] L.A. Sterczewski, J. Westberg, G. Wysocki, Computational coherent averaging for free-running dual-comb spectroscopy, Opt. Express 27 (2019) 23875–23893.
[28] Ł.A. Sterczewski, A. Przewłoka, W. Kaszub, J. Sotor, Computational Doppler-limited dual-comb spectroscopy with a free-running all-fiber laser, APL Photon. 4 (2019), 116102.
[29] Y. Wei, B. Li, X. Wei, Y. Yu, K.K.Y. Wong, Ultrafast spectral dynamics of dual-color-soliton intracavity collision in a mode-locked fiber laser, Appl. Phys. Lett. 112 (2018), 081104.
[30] S. Khorram, M.G. McInnis, E.M. Provost, Trainable timewarping: aligning time-series in the continuous-time domain, in: IEEE International Conference on Acoustics, Speech and Signal Processing, (2019), pp. 3502–3506.
[31] K. Kawano, T. Kutsuna, S. Koide, Neural time warping for multiple sequence alignment, in: IEEE International Conference on Acoustics, Speech and Signal Processing, (2020), pp. 3837–3841.
[32] Z. Tao, J. Zhang, J. You, H. Hao, H. Ouyang, Q. Yan, S. Du, Z. Zhao, Q. Yang, X. Zheng, T. Jiang, Exploiting deep learning network in optical chirality tuning and

manipulation of diffractive chiral metamaterials, Nanophotonics 9 (2020) 2945–2956.
[33] Z. Tao, J. You, J. Zhang, X. Zheng, H. Liu, T. Jiang, Optical circular dichroism engineering in chiral metamaterials utilizing a deep learning network, Opt Lett 45 (2020) 1403–1406.
[34] I.E. Gordon, L.S. Rothman, C. Hill, R.V. Kochanov, Y. Tan, P.F. Bernath, M. Birk, V. Boudon, A. Campargue, K. Chance, The HITRAN2016 molecular spectroscopic database, J. Quant. Spectrosc. Radiative Transf. 203 (2017) 3–69.
[35] C. Zeng, X. Liu, L. Yun, Bidirectional fiber soliton laser mode-locked by single-wall carbon nanotubes, Opt. Express 21 (2013) 18937–18942.
[36] T. Jiang, K. Yin, C. Wang, J. You, H. Ouyang, R. Miao, C. Zhang, K. Wei, H. Li, H. Chen, R. Zhang, X. Zheng, Z. Xu, X. Cheng, H. Zhang, Ultrafast fiber lasers mode-locked by two-dimensional materials: review and prospect, Photon. Res. 8 (2020) 78–90.
[37] E.J. Keogh, M.J. Pazzani, Derivative dynamic time warping in Proceedings of the 2001 SIAM international conference on data mining, (SIAM2001), pp. 1–11.
[38] D.P. Kingma, J.L. Ba, ADAM: A method for stochastioc optimization, in: International Conference on Learning Representations, (2015).
[39] A. Schliesser, M. Brehm, F. Keilmann, D.W. van der Weide, Frequency-comb infrared spectrometer for rapid, remote chemical sensing, Opt. Express 13 (2005) 9029–9038.